Biophysical Chemistry 5 (1976) 285–299

THE FLEXIBILITY OF LOW MOLECULAR WEIGHT DOUBLE-STRANDED DNA AS A FUNCTION OF LENGTH.
I. Isolation and physical characterization of seven fractions*

Jamie E. GODFREY**
Department of Polymer Research, The Weizmann Institute of Science, Rehovot, Israel, and Department of Biology, The Johns Hopkins University, Baltimore, Maryland 21218, USA

Received 4 December 1975

Sonicated calf thymus DNA was fractionated by rate zonal centrifugation into seven fractions with weight average molecular weights ranging from 0.28 to 1.3×10^6 daltons, as determined by sedimentation equilibrium and light scattering measurements (the latter are described in the accompanying paper). Electron microscopy and sedimentation equilibrium analysis revealed these fractions to be narrowly disperse with M_w/M_n ratios averaging about 1.06. Intrinsic viscosities and sedimentation rates were measured and found to vary linearly with molecular weight in double-logarithmic plots in fair agreement with previously published functions relating these parameters for low molecular weight DNA. The average value for β from the Mandelkern–Flory equation was 2.59×10^6, also agreeing with reported estimates of this parameter for short DNA. These data will be used in the second paper of this series to calculate the persistence length of the DNA fragments in each of the seven fractions by light scattering and hydrodynamic theories for the Kratky–Porod worm-like coil.

1. Introduction

The conformation of double-stranded DNA in solution has been the subject of active investigation for a number of years (see Bloomfield et al. [1] and Eisenberg [2] for recent surveys). Particular attention has been focused on estimating the flexibility of duplex DNA in view of the necessity, in nature, of packing very long DNA molecules into compact biological structures, such as the heads of bacterial phages and eukaryotic chromosomes. The question to be answered is whether duplex DNA can accommodate the restricted volumes of such structures without exceeding the limits of its inherent flexibility, or must it be folded beyond these limits by a concerted, energy expending process.

* This work was supported in part by Project No. 06-059-1 granted to the Weizmann Institute of Science under the Special International Research Program of the National Institutes of Health, U.S. Public Health Service.
** Recipient during the course of this research of a Postdoctoral Fellowship from the Muscular Dystrophy Associations of America, Inc., and a Weizmann Senior Fellowship.

A number of experimental approaches have been taken, both hydrodynamic and thermodynamic, to evaluate DNA "stiffness". Estimates from these methods usually are given as the persistence length, a, a measure of chain flexibility, of a Kratky–Porod [3] worm-like coil which would mimic the properties measured. Thus an estimate is only as good as the degree to which the Kratky–Porod model approximates the conformation of duplex DNA in solution; however, all evidence to date would seem to confirm the worm-like coil as a realistic analog [1,2]. In determining persistence lengths, light scattering has the advantage of measuring the root mean square radius, $\langle R^2 \rangle^{1/2}$, of particles unambiguously [1,4], and for particles of known contour length, this parameter uniquely defines a. For DNA molecules, the contour length can be calculated from the molecular weight (determined by any convenient method, including light scattering) and the mass per unit length, which has been well established for the B structure of DNA in aqueous solutions of simple salts [5,6].

Light scattering has been used by a number of workers to estimate the persistence length of DNA

[7–13], but the reported values vary widely. There are several potential sources of error in light scattering measurements of DNA which can significantly affect the determination of a [4,7,14]. Chief among these is the non-linearity of the scattering function, $P(\theta)^{-1}$, for large, stiff coils. Accurate determination of $\langle R^2 \rangle^{1/2}$ of such solutes requires scattering measurements at very small angles (θ) to the incident beam, a region of measurement unavailable to most commercial light scattering photometers (excluding the recent laser instruments). Since $P(\theta)^{-1}$ approaches linearity in the low θ range as the root mean square radius of the particle decreases, the problem is essentially eliminated if the DNA analyzed is in the molecular weight range below 1.5×10^6 daltons. Native duplex DNA molecules of this size have not in the past been available for study; instead, studies have been made on solutions of short fragments produced by sonic radiation of high molecular weight DNA [10,13]. Such samples, however, are invariably polydisperse. Light scattering measurements yield the solute weight average molecular weight; sedimentation equilibrium also determines, most accurately, the weight average molecular weight (under certain conditions the number average with equal accuracy). But it is the Z-average root mean square radius which is determined from light scattering. Thus, accurate assessment of the persistence length in a given DNA sample depends upon a thorough characterization of the sample polydispersity. Moreover, too broad a weight distribution, even if well characterized, cannot be easily analyzed because polydispersity, itself, increases the non-linearity of $P(\theta)^{-1}$ due to the differential scattering of long and short particles as a function of θ [14].

An additional source of error has been the failure until now to quantitatively evaluate the contribution of the optical anisotropy of DNA particles to the scattering intensities [4,14,16]. This correction as we have found can be significant for short fragments since its magnitude is inversely proportional to particle length [15], and the sensitivity of the persistence length to errors in the estimate of $\langle R^2 \rangle^{1/2}$ increases dramatically as the particle length decreases.

Work on the problem of DNA conformation began in this laboratory with the study of Cohen and Eisenberg [10,17–19] who examined the physical properties of several narrow weight fractions of sonicated calf thymus DNA in the 4.5×10^5 dalton range. An ancillary finding from these experiments was the indication that the persistence length of the particles based on light scattering measurements was 150–190 nm [10], considerably higher than most values recently reported by others [1]. The present study was motivated by a desire to remeasure the presistence length of short DNA molecules by light scattering, and also, by examining a number of well characterized fractions spanning a 4–5 fold molecular weight range, to determine whether flexibility changes with chain length. In addition, it was thought important that viscosities and sedimentation rates be measured in order that the flexibility of the particles could be estimated from hydrodynamic theory as well. These measurements would also allow the relationships between $[\eta]$, $s^\circ_{20,w}$, and molecular weight to be empirically determined in a DNA size range for which there have been few reliable data to date.

In this paper the isolation of several very narrowly disperse samples of sonicated calf thymus DNA in the 0.3 to 1.3×10^6 dalton range are described, along with their characterization as to average molecular weight, polydispersity and hydrodynamic parameters. In the accompanying paper [15], these data are used in conjunction with light scattering measurements, described therein, to evaluate the persistence length of the DNA in each of the weight fractions by several approaches.

2. Materials and methods

Chemicals were reagent grade and water was doubly glass distilled.

2.1. Calf thymus DNA

The calf thymus double-stranded DNA used in all experiments was a highly polymerized, detergent purified preparation, a gift from J. Pouyet (also used by Cohen and Eisenberg [18]). Its protein content as estimated by the method of Lowry [20] was $<0.5\%$, by weight; repeated extraction of a sample of the DNA with a chloroform–octanol mixture [21] after treatment with pronase [22] failed to reduce the measured protein content further. Solutions of DNA which had been fragmented by sonic radiation to the 0.4×10^6 dalton range (next section) were observed to undergo

a typical hypochromic transition in solvent B (see below) beginning at ca. 82°C with a T_m of 89.2°C; the hypochromicity, $\Delta\Sigma$, was 43.5% (i.e., OD_{259} increased 43.5% over its value at room temperature). These values compare favorably with those observed for unfragmented calf thymus DNA [17,23].

Stock solutions of DNA were maintained in a preserving solvent (solvent A) of 0.2 M NaCl, 10 mM EDTA, pH 7, with a few added drops of chloroform; these solutions were stored at 4°C and remained free from bacterial and fungal contamination for over two years [24]. For all experimental measurements, the DNA was first thoroughly dialyzed into 0.2 M NaCl, 2 mM EDTA, 2 mM Na-PO_4, pH 7 (solvent B), at 25°C.

The nucleotide molar extinction at 259 nm in 0.2M NaCl, 2 mM EDTA, pH 7 (solvent B minus phosphate) was determined from orthophosphate content estimates by the method of Morrison [25]. The calculated $\epsilon(P)^{1\,cm}_{259}$, 6430 (which did not change over a two-year period), is essentially identical to values previously measured for this DNA preparation [18].

2.2. Sonication

Fragmentation of DNA was effected in a Raytheon 10 kc/s magnetostrictive sonic oscillator (model DF 101, 220 W) [18]. Irradiations were performed at 7°C on 90 ml samples of DNA dissolved in solvent A at a concentration of 1 mg/ml; samples were thoroughly flushed beforehand with nitrogen.

2.3. Rate zonal fractionation

Based on the procedure of Halsall and Schumaker [26,27], conditions were found to effectively fractionate sonicated, low molecular weight DNA by rate zonal centrifugation [28] into narrow sedimentation rate distributions: these included a relatively shallow sucrose gradient (5 to 17%, w/v) and a low loading of DNA (40 mg, at 1 mg/ml) to minimize nonideality effects. Runs were made in the B-XV titanium rotor at 34000 rpm, a typical run lasting 27 hours; both a MSE Super 65 and a Beckman L2-65B preparative ultracentrifuge were used.

2.4. Sedimentation velocity (boundary analyses)

Estimations of sedimentation rate distributions in DNA solutions, useful in monitoring the sonic fragmentation and rate zonal fractionation processes, and for determining the weight average $s^\circ_{20,w}$ values for the seven DNA fractions of this study were made by the technique of sedimentation boundary analysis [29,30]. Analyses were carried out in a Beckman Model E analytical ultracentrifuge equipped with the electronic speed control, photoelectric scanner system, and multiplex accessory unit. The concentration of DNA used in the cells was not more than 0.03 mg/ml to avoid boundary self-sharpening effects due to the pronounced sedimentation rate versus concentration dependence [31,32]. Runs were made at 22–23°C and 32000–36000 rpm; cells were scanned at 265 nm at 16 or 32 min intervals. Data was analyzed by the procedure outlined by Schumaker and Schachman [29] with the aid of a Fortran IV computer program written in our laboratory by Dori Cwikel.

Weight average sedimentation rates were determined directly from the sedimentation rate profiles. The low cell loading concentrations employed made extrapolation to infinite dilution to obtain s° values unnecessary [33]; doubling the cell loading concentrations in a few test runs did not detectably decrease the measured sedimentation rates.

2.5. Sedimentation equilibrium

DNA fractions were analyzed at sedimentation equilibrium by the high-speed meniscus depletion method of Yphantis [34] in a Beckman Model E analytical ultracentrifuge equipped with the electronic speed control unit and Rayleigh interference optical system. The camera lens was focused on the two-thirds level of the cell to minimize the effects of Weiner skewing [34]. Each fraction was run at several cell loading concentrations in the range 0.1 to 1.0 mg/ml and a minimum of two rotor speeds between 5200 and 10000 rpm. The large AN-J rotor was used and temperature was maintained at 20.3°C during all runs. Sedimentation equilibrium was attained in 48 to 72 hours as evidenced by fringe pattern constancy over a period of 8 hours or more.

Interferograms were measured on a Nikon Profile Projector, Model 6C, microcomparator equipped with a 50X

projecting lens and electronically monitored x-y precision screws (I.K.L., Incorporated) with digital readouts. Further conditions followed in a typical run (e.g., cell loading volumes, cell blank corrections, fringe pattern measuring protocol) are described in detail elsewhere [35]. Data were analyzed by the Roark and Yphantis Fortran IV computer program [35,36]. Program estimates of concentrations in the first 0.8 mm of the column were less than 3 μ of fringe displacement in all experiments.

The specific density increment, $(\partial\rho/\partial c)_\mu$, was determined for solutions of sonicated DNA at concentrations of 0.6 and 1.0 mg/ml exhaustively dialyzed against solvent B. Densities were measured in a DMA 02C Precision Density Meter (Anton Paar K.G., Graz, Austria), a densimeter of the resonant oscillator type. DNA concentrations were determined from 259 nm absorbancies. $(\partial\rho/\partial c)_\mu$ was calculated to be 0.450, in satisfactory agreement with the value reported by Cohen and Eisenberg for DNA in 0.2 M NaCl [17]. The density of solvent B at 25°C was 1.0058 g/ml.

2.6. Viscometry

Viscosity measurements were made in a Zimm–Crothers low shear rotating cylinder viscometer [37] manufactured by Beckman Instruments. Two rotors were used which produced shear rates of approximately 2.0 and 0.4 s^{-1}, values which are substantially lower than the threshold value required to elicit non-newtonian behavior from the highest molecular weight DNA fraction measured in this study [38,39].

2.7 Electron microscopy

The DNA weight fractions were visualized in either an JEM 7a or a Philips 300 electron microscope at nominal magnifications of 15000–50000. Grids of dispersed DNA particles were prepared by the floating film method of Kleinschmidt [40] as modified by Herzberg [41] and stained with uranyl acetate [42]. Some fractions were photographed in the normal bright field mode while others were recorded in dark field. Magnifications were determined from photographs of diffraction grating replicas taken at the beginning and end of each series of DNA pictures.

Contour lengths of DNA molecules were measured with an Electronic Graphics Calculator (Numonics Corp., North Wales, Pa.) from magnified projected images (2″ × 2″ Leitz-Prado 250/500 projector) of electron micrographs. This instrument measures contour distances to an accuracy of ± 1 mm in 3 cm of traverse arm travel. The author is indebted to Dr. Dana Carroll of the Carnegie Institute of Embryology, Baltimore, Md. for the use of this instrument.

In addition to those mentioned above, a number of computer programs, designed by Allen Kakala of the Johns Hopkins Computer Centre, were used to facilitate the analysis of various data.

3. Basic equations for sedimentation equilibrium analysis

Evaluating the molecular weight moments of polydisperse, nonideal systems by sedimentation equilibrium presents certain theoretical difficulties; a number of approaches have been suggested [43–45] which attempt to minimize the inherent uncertainties. The DNA fractions of this study were analyzed by the method of Fujita [43] which is based on the following approximation:

$$M_{w\,app}^{-1} = M_w^{-1} + 2A_2^*(c_m + c_b)/2 + \ldots, \qquad (1)$$

where c_m and c_b refer to the concentrations (g/ml) at the meniscus and cell bottom, respectively, and $A_2^* = A_2(1+\Delta)$. A_2 is the second virial coefficient and Δ is a small correction which, for a given system, depends primarily on the polydispersity and rotor speed. $M_{w\,app}$ is defined as:

$$M_{w\,app} = \frac{2RT(\mathrm{d}\ln c_r/\mathrm{d}r^2)}{\omega^2(\partial\rho/\partial c)_\mu}$$

where R, T and ω have their conventional definitions; $(\partial\rho/\partial c)_\mu$ is the density increment at constant chemical potential for diffusible components (water and salt), and $(\mathrm{d}\ln c_r/\mathrm{d}r^2)$ is evaluated at $(c_m + c_b)/2$, as implied in eq. (1).

M_w^{-1} is found by the usual extrapolation to infinite dilution of a plot of $M_{w\,app}^{-1}$ versus c, where each reciprocal value is plotted at $(c_m + c_b)/2$. If higher virial terms are negligible, the slope will be linear and equal to $2A_2(1+\Delta)$. Δ is very small for narrowly polydispersed systems for which the cross-virial terms, A_{2ij}, are essentially equal; A_{2ij} then can be closely approximated by a single virial coefficient, A_2. If, however, the A_{2ij}'s

are not equal or if higher virial terms are finite, Δ will be larger and $M_{w\,app}^{-1}$ can be expected to be more sensitive to rotor speed. Insensitivity to ω^2 (i.e., reciprocal apparent weight average values at different speeds fall on the same extrapolant to M_w^{-1}) is a strong indication that the system can be described in terms of a single virial, A_2, and Δ is small; A_2^* would then closely approximate A_2.

Because the sedimentation equilibrium experiments were done under conditions of meniscus depletion, apparent number average molecular weights can be accurately evaluated from [34]:

$$M_{n\,app}^{-1} = \frac{2RTc_r}{\omega^2(\partial\rho/\partial c)_\mu} \Big/ \int_{r_m}^{r} c_r\, d(r^2),$$

where the denominator, the mass integral, is measured from the meniscus (zero concentration) to the radial position r, and c_r is the concentration at that point. The two-term virial expansion, analogous to eq. (1), for the number average molecular weight is:

$$M_{n\,app}^{-1} = M_n^{-1} + A_2^*(c_m + c_b)/2\,. \qquad (2)$$

M_n^{-1} and A_2^* are estimated by the plotting procedure described above.

4. Experimental results

4.1. Sonication and rate zonal fractionation of calf thymus DNA

Sonic radiation under the conditions employed breaks down high molecular weight DNA to a limiting size distribution with a weight average length of ca. 250 nm (fig. 1). As reported by other workers, it was found that prolonged irradiation worked only to sharpen the distribution somewhat with little increase in the concentration of lower molecular weight species [17,46,47].

A total of 800 mg of DNA sonicate was fractionated in 21 rate zonal centrifugation runs; a typical elution profile is shown in fig. 2. The large number of runs was necessary because, due to nonideality effects, only 35–45 mg of DNA could be effectively fractionated in one centrifugation. Fractions from the eluted peak

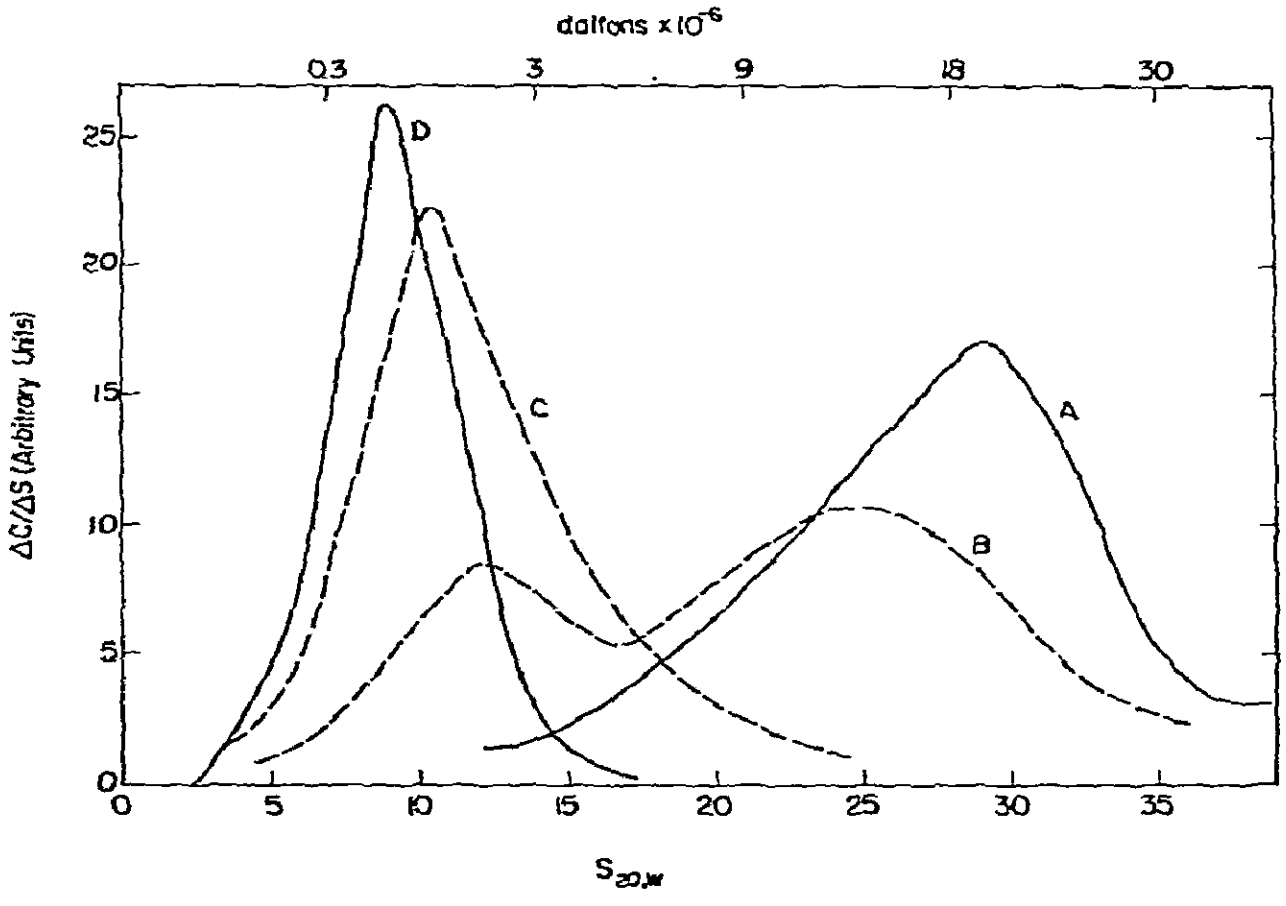

Fig. 1. Sedimenting boundary analyses of calf thymus DNA after different times of sonication (see section 2 for conditions). Curve A: Before sonication; curve B: after 15 min; curve C: after 30 min; curve D: after 1 hour. Molecular weight estimates based on the $s^\circ_{20,w}$ vs molecular weight relationship for double-stranded DNA of Eigner and Doty [24].

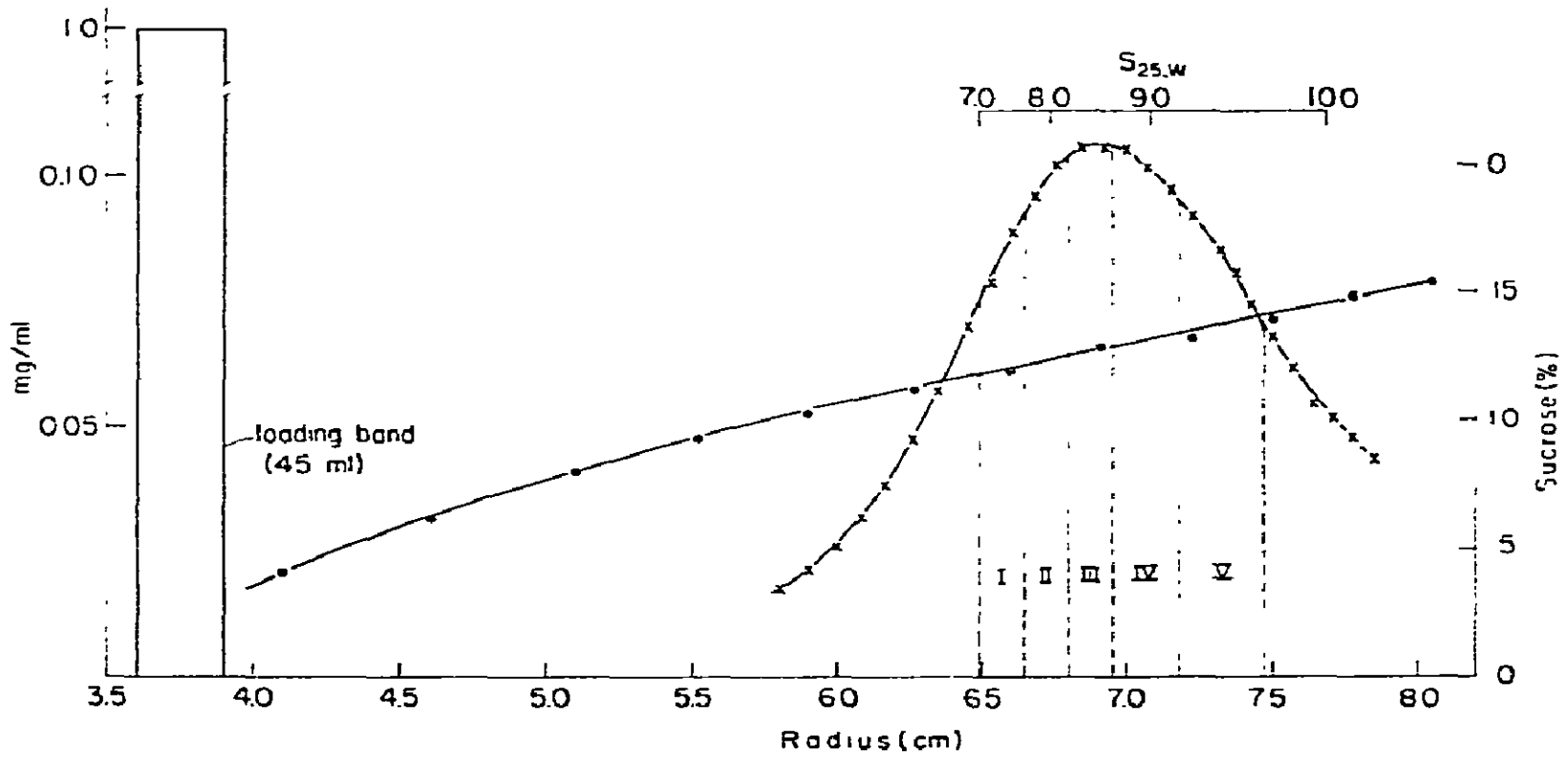

Fig. 2. Rate zonal centrifugation of sonicated calf thymus DNA: First fractionation of samples I–V. 45 mg of DNA sonicate in solvent A banded in a XV zonal rotor at the radial position shown and centrifuged at 34000 rpm for 28 hours at 12°C. DNA concentrations are based on 259 nm absorbancies, sucrose concentrations on refractive indices. 24 ml fractions (crosses) within Latin numerated divisions pooled from several runs to give fractions I–V (each subsequently recentrifuged; see text).

were analyzed be sedimentation boundary analysis, and on the basis of their sedimentation rate distributions, tubes from a series of runs were pooled to yield several weight class samples of 30–40 mg each. After concentrating by pelleting at 150000–250000 g, each concentrated sample was recentrifuged in the rate zonal rotor, the leading and trailing portions of the eluted peak discarded, and the center fractions pooled.

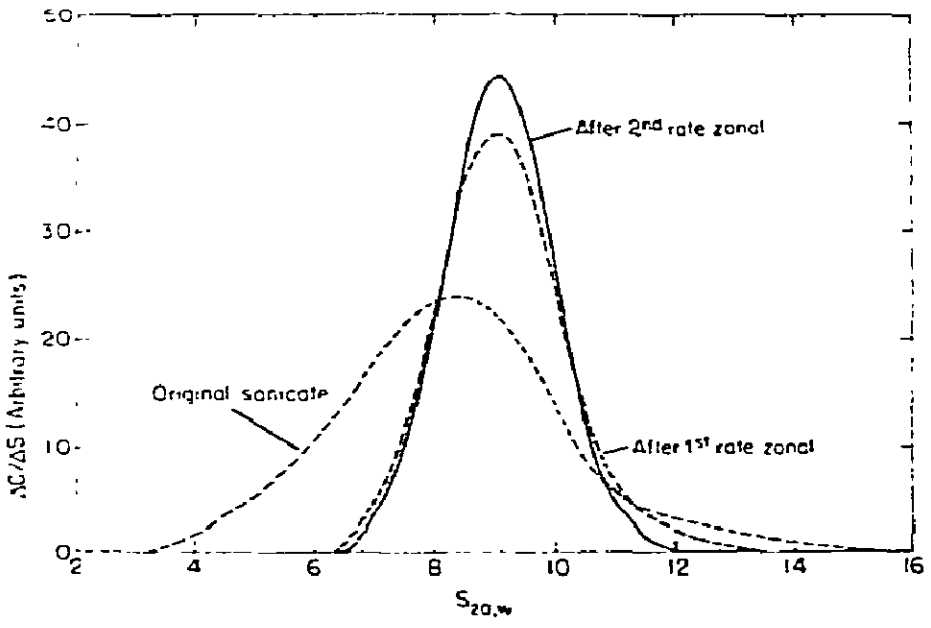

Fig. 3. Sedimenting boundary analysis of fraction V at three stages of isolation.

The samples were again dialyzed to rid them of sucrose and concentrated by pelleting, as above; the average yield per fraction was about 27 mg. Seven different weight class samples with weight average molecular weights ranging from 280000 to 1.3 million daltons were isolated in this way for subsequent characterization and analysis. Sedimentation boundary analyses of Fraction V at three stages of isolation are shown in fig. 3 (the effectiveness of the second rate zonal centrifugation in improving the distribution may, in fact, have been greater than these data would indicate, for reasons discussed later).

4.2. Sedimentation equilibrium

Fractions I through VI were analyzed by the high-speed meniscus depletion method [34] at several cell loading concentrations and two or more rotor speeds*. The downward curvature seen in the $\log c$ versus $r^2/2$ plot of data from Fraction IV (fig. 4a) demonstrates the pronounced nonideal behavior of the DNA fragments in solution; it is sufficient to override the effects

* Fraction VII could not be measured because solute packing on the cell bottom was observed at the lowest rotor speed which would effect meniscus depletion.

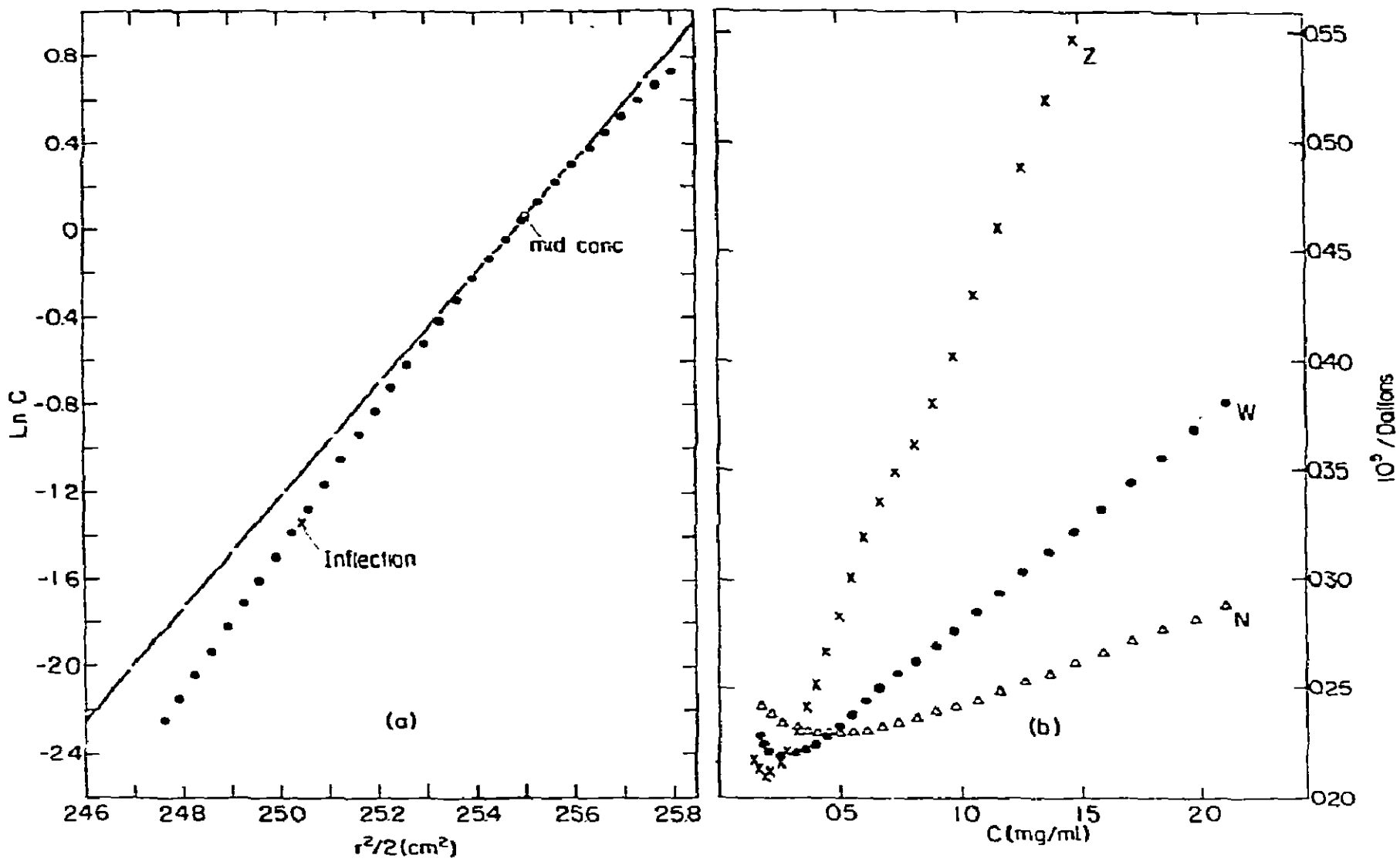

Fig. 4. Sedimentation equilibrium data from Fraction IV. (a) Ln c versus $r^2/2$ plot. Run conditions: 100 μl loading volume at 0.45 mg/ml in solvent B, 6000 rpm, 20.3°C. Data points generated by Roark–Yphantis computer program analysis [36]. Solid line is tangent to the data points at $(c_m - c_b)/2$ and its slope is proportional to $M^{-1}_{w\,app}$ at that concentration. (b) Apparent reciprocal number, weight, and Z-average molecular weights as a function of cell radial concentration; from Roark–Yphantis computer program analysis. Minimum in $M^{-1}_{w\,app}$ curve corresponds to inflection seen in ln c versus $r^2/2$ plot.

of polydispersity at concentrations above 0.25 mg/ml (inflection point). Analysis of the ln c versus r^2 curve by the Roark–Yphantis computer program [36] yields the reciprocal molecular weight averages as a function of radial solute concentration seen in fig. 4b. The minimum in this curve corresponding to the inflection point in the ln c versus r^2 function is a characteristic feature of $1/M_{app}$ versus c_r plots for nonideal solute systems at sedimentation equilibrium [34]. In fig. 5 the reciprocal molecular weight averages (number, weight, and Z) of Fraction IV are plotted as a function of the mid-point concentration in the cell (see section 3); each point is from a separate run at a particular cell loading concentration and rotor speed. Note that the mid-point molecular weight averages at the two rotor speeds fall on the same line. This independence from rotor speed was observed for all six fractions analyzed, as can be seen in fig. 6 where the $1/M_w$ versus c plots are given. It is particularly striking in the results from Fraction IV; for this fraction three rotor speeds were used spanning an almost two-fold difference in centrifugal field.

The extrapolated values at infinite dilution of M_n and M_w for the six fractions are listed in table 1; the limits are standard errors of estimate of the extrapolates. The weight average molecular weights obtained from the light scattering measurements described in the accompanying paper [15] are included for comparison. it can be seen that the values from the two methods differ by less than 3%. The second virial coefficients calculated from the concentration dependence of the number and weight average molecular weights

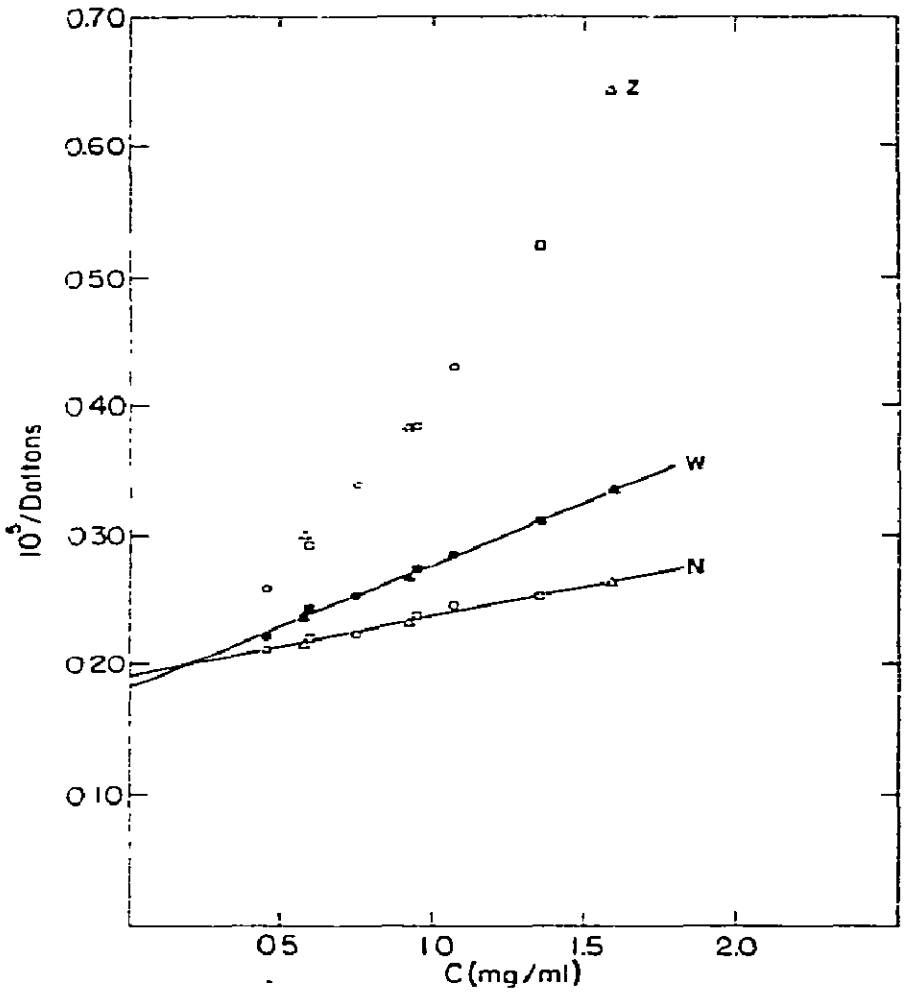

Fig. 5. Apparent reciprocal number, weight and *Z*-average molecular weights of Fraction IV: Mid-concentration values from runs at three rotor speeds and three cell loading concentrations. Circles: 6000 rpm; squares: 7200 rpm; triangles 8000 rpm. Extrapolations are by linear least squares fit.

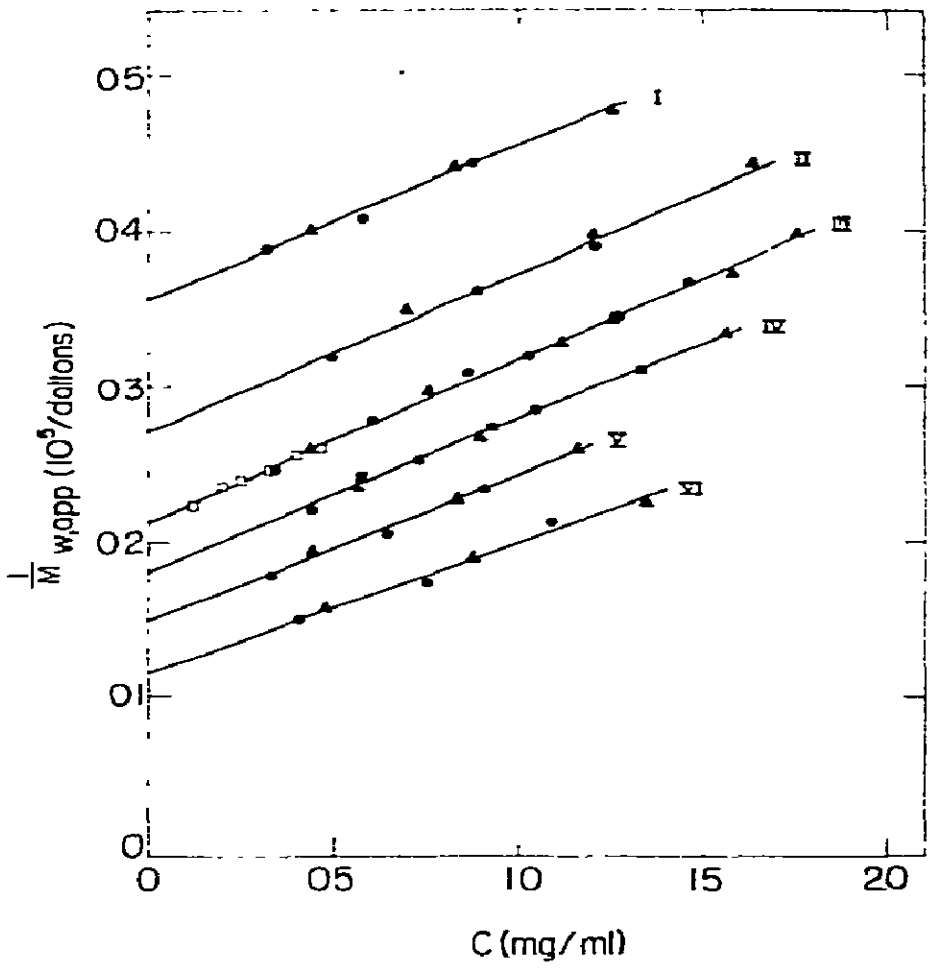

Fig. 6. Apparent reciprocal weight average molecular weight data from Fractions I–VI: Mid-concentration values at two or more rotor speeds and cell loading concentrations. Fraction I: (●) 8000 rpm; (▲) 10000 rpm. Fraction II: (●) 7200 rpm; (▲) 9000 rpm. Fraction III: (●) 6800 rpm; (▲) 8000 rpm (six cell loading concentrations at each speed). Fraction IV: (●) 6000 rpm; (▲) 7200 rpm; (■) 8000 rpm. Fraction V: (●) 5600 rpm; (▲) 6800 rpm. Fraction VI: (●) 5200 rpm; (▲) 6000 rpm. All experiments with 100 μl loading volume and at 20.3°C. Open squares are zero angle apparent reciprocal weight average molecular weights ($Kc/R_{\theta=0}$) from light scattering measurements of Fraction III described in the accompanying paper [15]. Extrapolations are by linear least squares fit.

(eq. 1 and 2) are listed in table 2; they are also in close agreement with the corresponding values obtained from light scattering. This agreement is illustrated in fig. 6 where the light scattering data points from Fraction III (open squares) are included and seen to fall on the extrapolated portion of the $1/M_w$ line.

4.3. Electron microscopy

Representative fields from Fractions I, V and VII are shown in fig. 7. The clarity of the particles in both light and dark field micrographs permitted precise contour length measurements. Rejection of particles due to clumping or of fields because of evident particle orientation was minimal. The lengths of over 640 particles from each fraction were measured and histograms compiled (fig. 8); the abscissas are in units of L/L_w to allow visual comparison of distribution widths.

Table 1 lists the weight and number average molecular weights tabulated for the seven fractions (assuming 1950 daltons/nm for the sodium salt). Considerable divergence can be noted between the molecular weight values obtained from contour length measurements and those from sedimentation equilibrium or light scattering. Table 1 lists M_w/M_n ratios determined from the histograms, and these can be compared with their corresponding values obtained from sedimentation equilibrium. Here too, discrepancies between the two sets of figures are evident; the disagreement is most pronounced between the values for the low molecular weight fractions, I–III. Reasons for the lack of agreement between the electron microscopy data and that

Table 1
Weight and number average molecular weights and their ratios

Fraction	Weight average molecular weight ($\times 10^{-5}$)				Number average molecular weight ($\times 10^{-5}$)		Weight average/ Number average	
	L.S.[a]	S.E.[b]	Average of L.S. + S.E.	E.M.[c]	S.E.[b]	E.M.[c]	S.E.[b]	E.M.[c]
I	2.82 ± 0.03	2.80 ± 0.03	2.81	2.25	2.73 ± 0.06	2.10	1.03	1.07
II	3.56 ± 0.03	3.69 ± 0.07	3.62	3.09	3.60 ± 0.11	2.87	1.02	1.08
III	4.63 ± 0.04	4.70 ± 0.07	4.67	4.19	4.46 ± 0.08	4.01	1.05	1.04
IV	5.29 ± 0.05	5.51 ± 0.07	5.40	4.71	5.22 ± 0.06	4.45	1.05	1.06
V	6.49 ± 0.06	6.65 ± 0.11	6.57	6.27	6.32 ± 0.17	6.04	1.05	1.04
VI	8.26 ± 0.04	8.65 ± 0.32	8.46	8.43	7.80 ± 0.36	7.84	1.11	1.07
VII	12.69 ± 0.04	–[d]	12.69	11.04	–[d]	10.02	–[d]	1.10

a) From light scattering (see second paper of this series [15]); average of values at 436 and 546 nm incident light. Limits are standard errors of estimate of the linear least squares extrapolations.
b) From sedimentation equilibrium. Limits are standard errors of estimate of the linear least squares extrapolations (weight average molecular weights: fig. 6; number average molecular weight extrapolation, shown for Fraction IV only: fig. 5).
c) From electron microscopy; based on contour length histograms (fig. 8) assuming 1950 daltons/nm for the sodium salt of double-stranded DNA.
d) Fraction VII not measured by sedimentation equilibrium; see footnote, p. 6.

Table 2
Hydrodynamic parameters and second virial coefficients

Fraction	L_w (nm)[a] (average of L.S. and S.E.)	$s_{25,s}$[b]	$s_{20,w}$[c]	$[\eta]$ (dl/g)[d]	k[e]	β ($\times 10^{-6}$)[f]	A_2 (L.S.) (mole ml/g^2 $\times 10^4$)[g]	A_2^*(S.E.) (mole ml/g^2 $\times 10^4$)[h]
I	144	7.79	7.16	1.52 ± 0.05	1.09	2.55	5.88	5.21
II	186	8.34	7.67	2.32 ± 0.02	0.41	2.65	5.64	5.13
III	239	8.89	8.18	2.92 ± 0.02	0.48	2.57	4.69	5.18
IV	277	9.36	8.60	3.66 ± 0.06	0.50	2.65	5.83	4.84
V	337	9.80	9.01	4.69 ± 0.02	0.36	2.65	5.51	4.64
VI	434	10.38	9.54	5.82 ± 0.02	0.29	2.55	5.12	4.45
VII	651	11.73	10.78	8.91 ± 0.08	0.27	2.53	4.18	–[i]
						Ave. 2.59		

a) Weight average contour lengths from average of light scattering [15] and sedimentation equilibrium molecular weights (column 4, table 1), assuming 1950 daltons/nm for the sodium salt of double-stranded DNA.
b) Weight average sedimentation coefficients in solvent B at 25°C; used in calculation of β. $\rho_s \approx 1.0058$ g/ml at 25°C.
c) Weight average sedimentation coefficients corrected to water at 20°C assuming a value for $(\partial\rho/\partial c)_\mu$ of 0.450.
d) Intrinsic viscosities at 25°C; used in calculation of β. Limits are standard errors of estimate of the linear least squares extrapolations (fig. 11).
e) Huggins' constants.
f) Mandelkern–Flory parameters; in solvent B at 25°C.
g) Second virial coefficients from light scattering [15].
h) Apparent second virial coefficients from sedimentation equilibrium (eq. 1 and 2).
i) See footnote d), table 1.

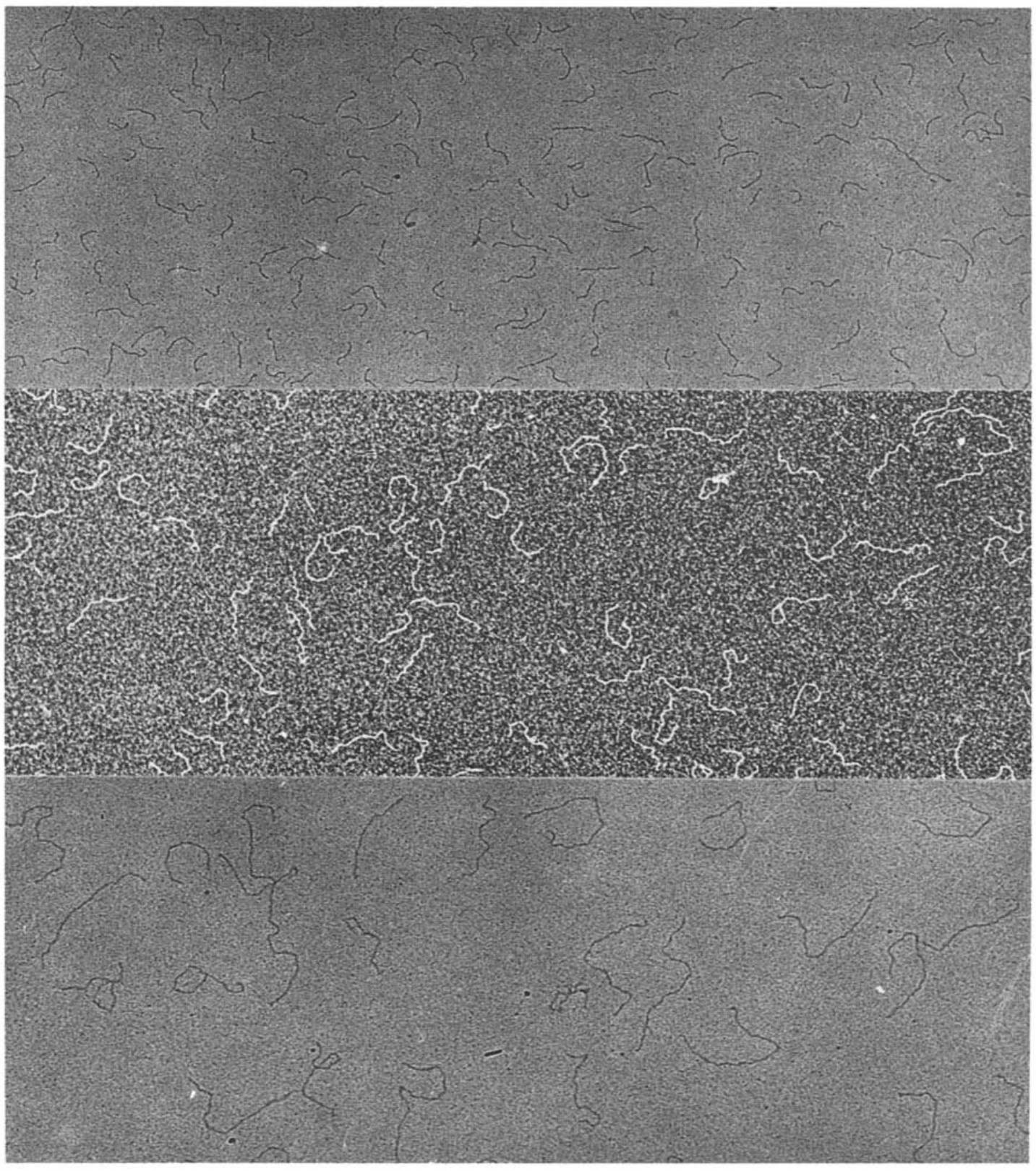

Fig. 7. Representative electron micrograph fields of Fractions I, V, and VII. Particles are positively stained with uranyl acetate. Fractions I (top) and VII (bottom) are in light field mode, Fraction V in dark field. (Magnification: 40000×.)

obtained from light scattering and sedimentation equilibrium will be considered later.

4.4. Sedimentation velocity

The sedimenting boundaries of the seven fractions at a concentration of 0.03 mg/ml were analyzed to determine the apparent distribution of sedimenting species present. At this low loading concentration, the measured s differs insignificantly from s° (see section 2). Although the diffusion coefficient of DNA molecules – even of short fragments – is low, it was evident that diffusion and perhaps convective disturbances, as well, acted to significantly broaden the sedimenting boundary. For these reasons, the boundary profiles do not reflect the true (narrower) distributions of

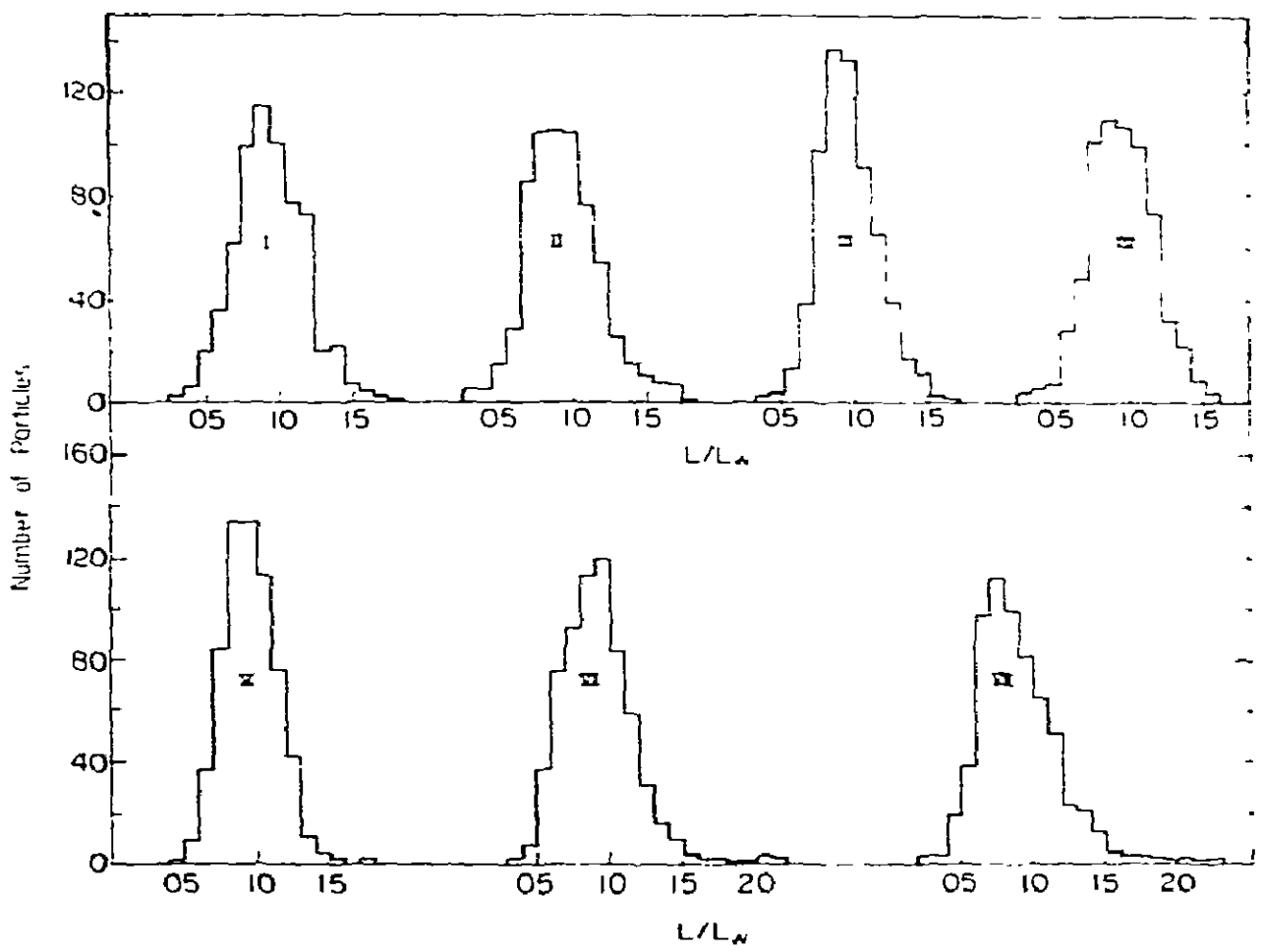

Fig. 8. Contour length histograms of Fractions I–VII from electron micrograph measurements. Abscissa is in units of L/L_N to facilitate comparison of distributions. 640–670 particles from each fraction were measured.

species present in the fractions. Fig. 9 illustrates the discrepancy between the molecular weight distributions of Fraction V determined from sedimenting boundary analysis and contour length measurements. [Conversion of apparent $s^{\circ}_{20,w}$ values to molecular weights was based upon the empirical relationship between these two parameters for short DNA fragments derived in this study (eq. 4).]

Weight average $s^{\circ}_{20,w}$'s for the seven fractions, however, were calculated from the apparent sedimentation rate distributions since the weight average s values of narrowly polydispersed systems are affected only negligibly by modest diffusion. For this purpose the two boundaries of each fraction which were recorded the longest time after t_0, while a true plateau centrifugal to the boundary still existed, were analyzed and their profiles averaged. These late boundaries were chosen because the broadening effect on the distributions from diffusion continually decreases throughout sedimentation due to the different time dependencies of the two transport processes [45]. The calculated weight average s°'s were essentially coincident with the values at the maximum in the (dc/ds) versus s° plots, as expected for narrowly dispersed mixtures. The usual buoyancy and viscosity corrections were applied to convert the calculated weight average sedimentation rates to $s^{\circ}_{20,w}$'s (table 2).

4.5. Viscosity

The viscosities of the seven fractions were determined at room temperature in a Zimm–Crothers low shear viscometer; five or more concentrations of each fraction were measured, except in the case of Fraction I where loss of material restricted the measurements to three. The reduced viscosities ($\eta_{sp/c}$) plotted against concentration are seen in fig. 10. Extrapolation of the linear least squares fitted lines to infinite dilution yielded the intrinsic viscosities, and from the relation:

$$\eta_{sp/c} = [\eta] + kc[\eta]^2,$$

the Huggins constant, k, was calculated. The two parameters for each of the seven fractions are listed in table 2. Because of the narrow concentration range

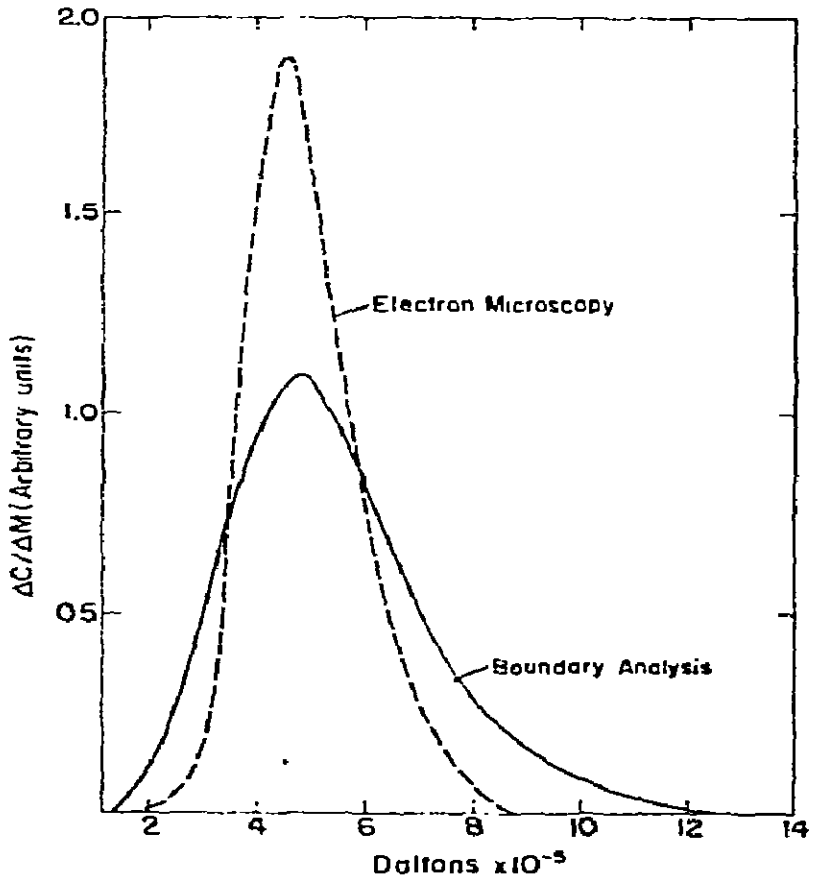

Fig. 9. Molecular weight distribution of Fraction III from sedimenting boundary analysis and electron microscopy. Electron microscopy distribution is smoothed approximation of length histogram (fig. 8). Particle lengths converted to molecular weights by assuming 1950 daltons/nm for the sodium salt of double-stranded DNA. $s^{\circ}_{20,w}$'s converted to molecular weights by eq. (4).

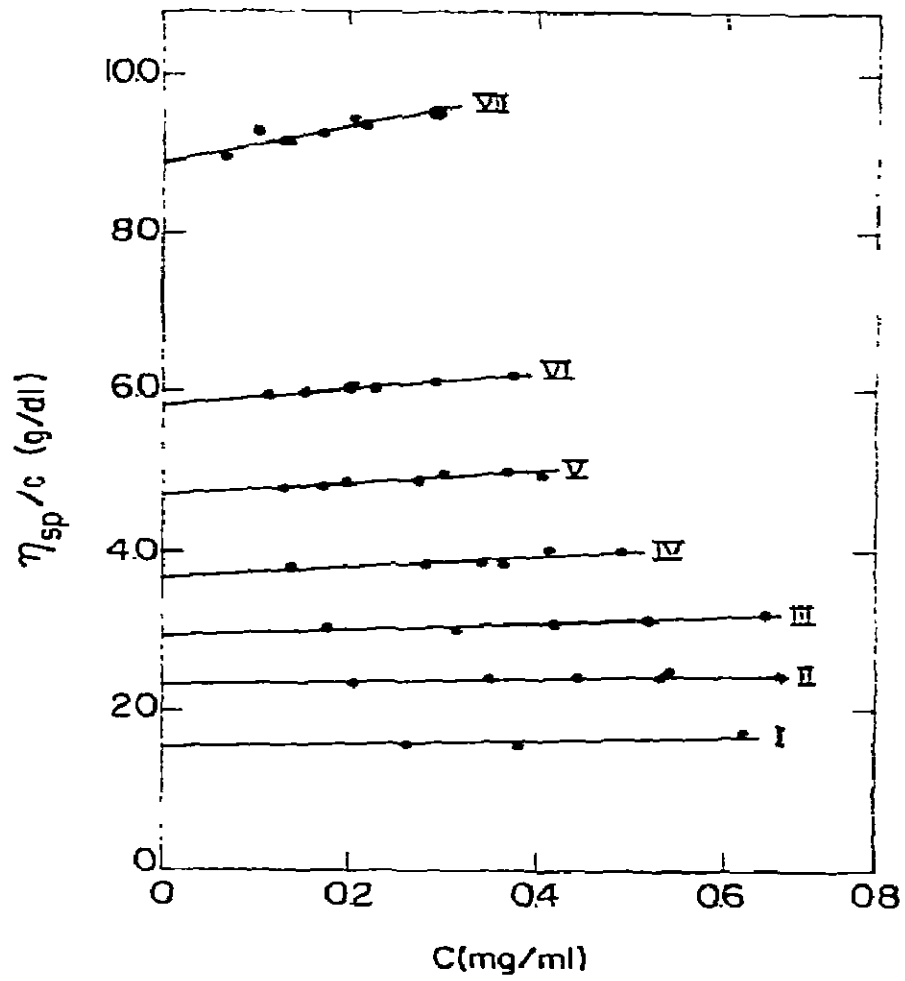

Fig. 10. Reduced viscosities of Fractions I–VII. Extrapolations to intrinsic viscosities ($[\eta]$) by linear least squares regression analysis. Large data point, Fraction VII: Measured a year after other data points; fraction kept cold in solvent A during interim.

spanned by the viscosity measurements, the Huggins constant estimates should be considered as only approximate.

4.6. Correlations between M_w, $[\eta]$, and $s^{\circ}_{20,w}$

The relationships between the molecular weight of duplex DNA and its intrinsic viscosity and sedimentation rate have been the subject of much investigation [24,31,32,38,49–51]. Equations correlating M_w to the parameters usually take the general form,

$$\left\{ \begin{matrix} s^{\circ}_{20,w} \\ [\eta] \end{matrix} \right\} + b = KM^{a}$$

and give straight lines in double-logarithmic plots over a limited molecular weight range. It has proven difficult to formulate single expressions which satisfactorily relate M to either $[\eta]$ or $s^{\circ}_{20,w}$ over the whole molecular weight range for which data are available [24,51]. The problem is more acute at the low molecular weight end of the scale due, in part, to the paucity of reliable data in this region and perhaps also to the fact that, as DNA becomes shorter, it undergoes a shape change from a worm-like coil to a flexible rod [31,51].

The molecular weights and the corresponding values for $[\eta]$ and $s^{\circ}_{20,w}$ of the seven fractions of this study are best related by:

$$[\eta] + 1.2 = (0.515 \pm 0.013) \times 10^{-4} M_w^{0.867}, \qquad (3)$$

$$s^{\circ}_{20,w} = (0.265 \pm 0.002) M_w^{0.270}. \qquad (4)$$

The limits are standard errors of estimate of the linear least squares lines fitted to the points in log–log plots (fig. 11). Also included in fig. 11 are analogous functions reported by other workers for double-stranded DNA applicable to the low molecular weight range.

The molecular weights, intrinsic viscosities, and sedimentation coefficients can be combined in the

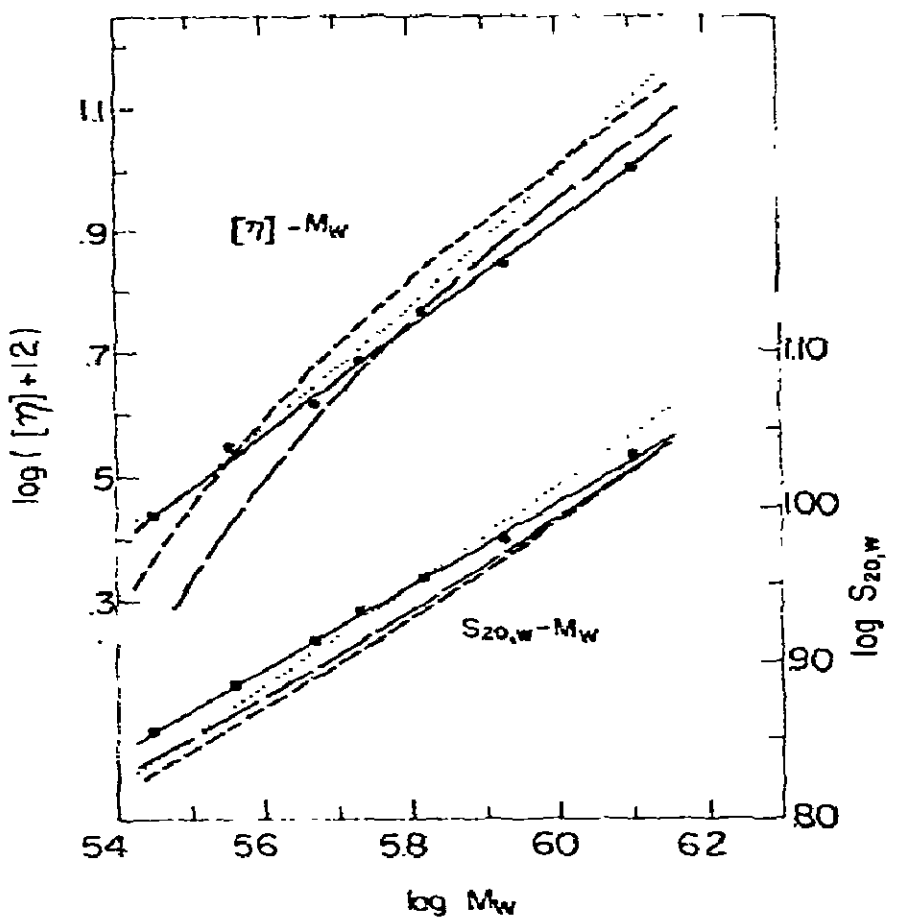

Fig. 11. Double logarithmic plots of intrinsic viscosities and sedimentation coefficients versus weight average molecular weights of fractions I–VII. Points are the seven fractions; solid line is the linear least squares line fitted to the points. Other lines are $[\eta]$ or $s^{\circ}_{20,w}$ vs M_w functions appearing in the literature: dotted lines are from Eigner and Doty [24]; short dashed lines are from Reinert et al. [49]; long dashed lines are from Crothers and Zimm [31].

familiar Mandelkern–Flory equation [52] which yields the mildly shape-sensitive parameter β:

$$\beta = \frac{s^{\circ}_{25,0}[\eta]^{1/3}\eta_0 N_A}{10^{13} M_w^{2/3}(\partial\rho/\partial c)_\mu},$$

where $s^{\circ}_{25,0}$, $[\eta]$, (in dl/g), η_0 (solvent viscosity, 0.0092 P), and $(\partial\rho/\partial c)_\mu$ are measured in solvent B at 25°C. The β's for the individual fractions are listed in table 2 (along with the $s^{\circ}_{25,0}$ values used in these calculations). The average, 2.59×10^6, is in good agreement with both experimental and theoretical values for double-stranded DNA within the molecular weight range of the fractions characterized in this study [24, 53–55].

5. Discussion

Analysis of the sedimenting boundaries of the fractions at different times revealed that the apparent distribution of sedimentation coefficients is significantly broadened by diffusion and very likely convection as well. From Fick's second law it follows that the narrower the distribution, the greater will be the boundary spreading due to diffusional transport. It is reasonable to conclude, therefore, that the improvement in the distribution of Fraction V after the second rate zonal fractionation step (fig. 3) is probably better than shown because of the greater diffusional spreading experienced by this boundary than by the boundary of the broader distribution from the first fractionation. Moreover, in view of the above, the length distributions determined from electron microscopy rather than the sedimenting profiles were used where necessary in the conformational analyses to corrent for the effects of polydispersity (cf. fig. 9).

However, the distributions of the fractions determined from contour measurements are themselves subject to at least two sources of error, which become more pronounced with decreasing particle length. One is the imprecision in the measuring process which is significant for the shorter fragment fractions whose magnified particles were of the order of 1.5 to 3 cm in length. The second error arises from the fact that electron microscope grid surfaces are not uniformly flat so that molecules inclined to the horizontal measure shorter by a factor equal to the cosine of the angle of inclination. Again this source of error is greater for the lower weight fractions whose particles are more readily confined throughout their length to tilted surface areas. That both errors affected the size distributions obtained from contour length measurements can be inferred from the poor agreement between the L_w/L_n ratios derived from the particle length histograms and from sedimentation equilibrium (table 1). Those determined by the latter method are generally lower in value with the differences between the values by the two techniques being greatest for Fractions I and II, as expected.

A much larger discrepancy was found between the weight average lengths of the fractions determined from the contour measurements and those from both light scattering and sedimentation equilibrium (assuming the B structure for DNA in solution [5,6]). These differences are likely due to particle shrinkage during the staining and drying steps of electron microscope grid preparation [51,56] and the second source of error mentioned above. The lack of agreement is

greatest for the lower weight fractions, perhaps because the short particles of these samples, with fewer attachment points to the grid surface can more easily respond to shrinkage forces.

On the other hand, there was close agreement between the weight average molecular weights obtained from light scattering and sedimentation equilibrium; the average difference between the two sets of values for Fractions I–VI (VII was not measured by sedimentation equilibrium) was $< 3\%$. The second virial coefficients obtained for Fractions I–VI from light scattering are in close agreement with the apparent values, A_2^*, from sedimentation equilibrium (to within 10%, or, if the M_w's from the two methods are normalized, to within 7%). Moreover, the $M_{n\,app}^{-1}$ and $M_{w\,app}^{-1}$ versus c plots are linear, thus giving no hint of virial terms higher than the second for short DNA particles in the solvent system used. Both the slope and extrapolated reciprocal molecular weights are independent of rotor speed, at least within the range utilized for each fraction. These results suggest that contributions from cross-term virial effects to the non-ideal behavior of these mixtures are minimal and that the extrapolated $M_{w\,app}^{-1}$ and $M_{n\,app}^{-1}$ values at infinite dilution are very close to their true values. (A detailed treatment of these data from the point of view of analyzing polydisperse, nonideal systems by sedimentation equilibrium will be the subject of a separate communication.)

It was stated earlier that the flexibility of short duplex DNA fragments can be determined with confidence only from the analysis of samples which have been "well characterized" as to average molecular weight and polydispersity. The data presented herein suggest that this criterion has been met for the seven fractions isolated. Fig. 11 perhaps best illustrates this conclusion where it is seen that the data points defining the two functions relating $s^{\circ}_{20,w}$ and $[\eta]$ to M_w have standard errors of estimate of ca. 1 and 2%, respectively. This internal consistency among the data is also reflected by the narrow range of values calculated for the Mandelkern–Flory parameter, β, the average value of which, 2.59×10^6, agrees with theoretical estimates and previously published values for DNA in the low molecular weight range [24,49,54,55]. Confidence in the molecular weight values is further justified by the close agreement between the results from light scattering and sedimentation equilibrium – this despite the inherent difficulties in obtaining accurate estimates by these methods on highly nonideal behaving mixtures. Lastly, the narrowness of the length distributions (average $M_w/M_n \approx 1.06$) makes corrections to calculations of molecular conformation due to polydispersity relatively minor.

Acknowledgement

The author wishes to thank Dori Cwikel for her expert technical assistance and computer analyses of much of the data. He also thanks Dr. Robert Josephs for the electron micrographs and, in particular, for the dark field pictures of Fractions III and V which were entirely his work.

References

[1] V.A. Bloomfield, D.M. Crothers and I. Tinoco, Physical Chemistry of Nucleic Acids, (Harper and Row, New York, 1974) ch. 5.
[2] H. Eisenberg, in: Basic Principles in Nucleic Acids, Vol. 2, ed. P.O.P. Ts'o (Academic Press, New York, 1974) p. 171.
[3] O. Kratky and G. Porod, Rec. Trav. Chim. 68 (1949) 1106.
[4] H. Eisenberg, in: Procedures in Nucleic Acids, Vol. 2, eds. G.H. Cantoni and D.R. Davies (Harper and Row, New York, 1971) p. 137.
[5] J.D. Watson and F.H.C. Crick, Nature 171 (1953) 737.
[6] M.H.F. Wilkins, J. Chim. Phys. 58 (1961) 891.
[7] J.B. Hays, M.E Magar and B.H Zimm, Biopolymers 8 (1969) 531.
[8] E.P. Geiduschek and A.H. Holtzer, Adv. Biol. Med. Phys. 6 (1958) 431.
[9] P. Sharp and V.A Bloomfield, Biopolymers 6 (1968) 1201.
[10] H. Eisenberg, Biopolymers 8 (1969) 545.
[11] B.R. Jennings and H. Plummer, Biopolymers 9 (1970) 1361.
[12] J.R. Dawson and J.A. Harpst, Biopolymers 10 (1971) 2499.
[13] D.I Jolly and H. Eisenberg, Biopolymers, 15 (1976) 61.
[14] C.W. Schmid, F.A. Rinehart and J.E. Hearst, Biopolymers 10 (1971) 883.
[15] J.E. Godfrey and H. Eisenberg, Biophys. Chem. 5 (1976) 301.
[16] G. Weill, C. Hornick and S. Stoylov, J. Chim. Phys. 64 (1968) 12.
[17] G. Cohen and H. Eisenberg, Biopolymers 4 (1966) 429.
[18] G. Cohen and H. Eisenberg, Biopolymers 6 (1968) 1077.
[19] G. Cohen and H. Eisenberg, Biopolymers 8 (1969) 45.

[20] O.H. Lowry, N.J. Rosebrough, A.L. Farr and R.J. Randall, J. Biol. Chem. 193 (1951) 265.
[21] J. Marmur, J. Mol. Biol. 3 (1961) 208.
[22] F. Doppler-Bernardi and G. Felsenfeld, Biopolymers 8 (1969) 733.
[23] J. Marmur and P. Doty, J. Mol. Biol. 5 (1962) 109.
[24] J. Eigner and P. Doty, J. Mol. Biol. 12 (1965) 549.
[25] W.R. Morrison, Anal. Biochem. 7 (1964) 218.
[26] V.N. Schumaker and H.B. Halsall, Nature 221 (1969) 772.
[27] H.B. Halsall and V.N. Schumaker, Anal. Biochem. 30 (1969) 368.
[28] N.G. Anderson and E. Rutenberg, Anal. Biochem. 21 (1967) 259.
[29] V.N. Schumaker and H.K. Schachman, Biochim. Biophys. Acta 23 (1957) 628.
[30] V.N. Schumaker, E.G. Richards and S.T. Freer, J. Mol. Biol. 12 (1965) 517.
[31] D.M. Crothers and B.H. Zimm, J. Mol. Biol. 12 (1965) 525.
[32] P. Doty, B.B. McGill and S.A. Rice; Proc. Natl. Acad. Sci. U.S.A. 44 (1958) 432.
[33] F.W. Studier, J. Mol. Biol. 41 (1969) 189.
[34] D.A. Yphantis, Biochemistry 3 (1964) 297.
[35] J.E. Godfrey and W.F. Harrington, Biochemistry 9 (1970) 894.
[36] D.E. Roark and D.A. Yphantis, Ann. N.Y. Acad. Sci. 164, art. 1, (1969) 245.
[37] B.H. Zimm and D.M. Crothers, Proc. Natl. Acad. Sci. U.S.A. 48 (1962) 905.
[38] A. Prunell and G. Bernardi, J. Biol. Chem. 248 (1973) 3433.
[39] H. Eisenberg, J. Polymer Sci. 25 (1957) 257.
[40] A.K. Kleinschmidt and R.K. Zahn, Z. Naturforsch. 146 (1959) 770.
[41] M. Herzberg, personal communication.
[42] R.W. Davis and N. Davidson, Proc. Natl. Acad. Sci. U.S.A. 60 (1968) 243.
[43] H. Fujita, J. Phys. Chem. 73 (1969) 1759.
[44] D.A. Albright and J.W. Williams, J. Phys. Chem. 71 (1967) 2780.
[45] H. Utiyama, N. Tagata and M. Kurata, J. Phys. Chem. 73 (1969) 1448.
[46] A.R. Peacocke and N.J. Pritchard, Biopolymers 6 (1968) 605.
[47] N.J. Pritchard and A.R. Peacocke, Biopolymers 4 (1966) 259.
[48] H.K. Schachman, Ultracentrifugation in Biochemistry (Academic Press, New York, 1959) p. 135.
[49] K.E. Reinert, H. Triebel and J. Strassburger, Biochim. Biophys. Acta 287 (1972) 367.
[50] S.B. Leighton and I. Rubenstein, J. Mol. Biol. 46 (1969) 313.
[51] D. Freifelder, J. Mol. Biol. 54 (1970) 567.
[52] L. Mandelkern and P.J. Flory, J. Chem. Phys. 20 (1952) 212.
[53] K.E. Reinert, K.E. Strassburger and H. Triebel, Biopolymers 10 (1971) 285.
[54] O.B. Ptitsyn and Ye.Yu. Eizner, Vysokomol. Soyedin. 3 (1961) 1963.
[55] Ye.Yu. Eizner and O.B. Ptitsyn, Vysokomol. Soedin. 4 (1962) 1725.
[56] R.B. Inman, J. Mol. Biol. 25 (1967) 209.